Science of the Total Environment 752 (2021) 141786

Contents lists available at ScienceDirect

Science of the Total Environment

journal homepage: www.elsevier.com/locate/scitotenv

# The influences of phytoplankton species, mineral particles and concentrations of dispersed oil on the formation and fate of marine oil-related aggregates

Ingrid A. Henry, Roman Netzer, Emlyn Davies, Odd Gunnar Brakstad *

*SINTEF Ocean AS, Environment and New Resources, Trondheim, Norway*

## HIGHLIGHTS

- Oil-related aggregates were formed with phytoplankton, mineral particles and dispersed oil.
- Aggregate formations and sizes varied between phytoplankton species.
- Particle sizes were increased by low, but reduced by high mineral particle concentrations.
- Aggregation required dispersed oil concentrations of 1 mg/L or more.
- Oil compound groups sorbed to marine particles also at low oil concentrations.

## GRAPHICAL ABSTRACT

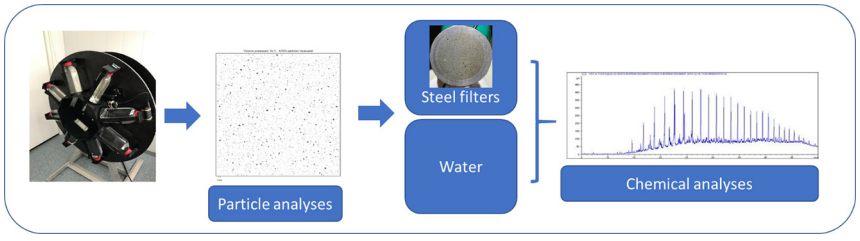


## ARTICLE INFO

*Article history:*
Received 20 June 2020
Received in revised form 12 August 2020
Accepted 17 August 2020
Available online 22 August 2020

Editor: Frederic Coulon

*Keywords:*
Dispersed oil
Phytoplankton
Mineral particles
Aggregation
Marine snow

## ABSTRACT

The formation and fallout of oil-related marine snow have been associated with interactions between dispersed oil and small marine particles, like phytoplankton and mineral particles. In these studies, the influences of phytoplankton species, mineral particle concentration, and oil concentration on the aggregation of oil in seawater (SW) were investigated. The experiments were performed in a low-turbidity carousel incubation system, using natural SW at 13 °C. Aggregation was measured by silhouette camera analyses, and oil compound group distribution and depletion by gas chromatography (GC-FID or GC–MS). Aggregates with median sizes larger than 500 μm in diameter were measured in the presence of dispersed oil and the phytoplankton species *Thalassiosira rotula*, *Phaeocystis globosa*, *Skeletonema pseudocostatum*, but not with the microalgae *Micromonas pusilla*. When mineral particles (diatomaceous earth) were incubated at different concentrations (5–30 mg/L) with dispersed oil and *S. pseudocostatum*, the largest aggregates were measured at the lower mineral particle concentration (5 mg/L). Since dispersed oil rapidly dilutes in the marine water column, experiments were performed with oil concentrations of from 10 mg/L to 0.01 mg/L in the presence of *S. pseudocostatum* and diatomaceous earth. Aggregates larger than 500 μm was measured only at the highest oil concentrations (10 mg/L). However, oil attachment to the marine particles were also measured at low oil concentrations (≤1 mg/L). Depletion of oil compound groups (*n*-alkanes, naphthalenes, PAHs, decalins) were measured at all oil concentrations, both in aggregate and water phases, with biodegradation as the expected main depletion process. These results showed that oil concentration may be important for oil-related marine snow formation, but that even oil droplets at low concentrations may attach to the particles and be transported by prevailing currents.



* Corresponding author at: SINTEF Ocean AS, Postboks 4762 Torgarden, 7465 Trondheim, Norway.
*E-mail address:* odd.g.brakstad@sintef.no (O.G. Brakstad).

https://doi.org/10.1016/j.scitotenv.2020.141786

## 1. Introduction

The formation and fate of aggregates associated with oil spills, often called marine oil snow (MOS) or Marine Oil Snow Sedimentation & Flocculent Accumulation (MOSSFA), has received considerable attention after the Deepwater Horizon (DWH) oil spill (Passow et al., 2012; Ziervogel et al., 2012; Daly et al., 2016; Passow, 2016). These processes were used to explain why considerable amounts of the Macondo oil were sedimented on the seabed during the oil spill (Valentine et al., 2014; Stout and Payne, 2016). Marine snow (MarS) comprises an important natural process, transporting particulate organic carbon to deep waters and seabeds (Alldredge and Silver, 1988; De La Rocha and Passow, 2007). The particles are associated with phytoplankton producing extracellular transparent exopolymer particles (TEP), "gluing" the particles into macrosopic aggregates >0.5 mm in diameter (Alldredge et al., 2002; Smetacek, 1985; van Eenennaam et al., 2016). Algal TEP can be formed by both diatoms and flagellates, and TEP production has been shown to vary between phytoplankton species grown in batch cultures (Passow, 2002).

In coastal seawater (SW), dispersed oil may also interact with suspended mineral particles in the water column, often of terrestrial origin from river effluents. Oil droplets and mineral particles may collide and form oil-mineral aggregates (OMAs), which have been shown to prevent re-coalescence of oil droplets and stabilizes small droplets, thus introducing beneficial conditions for oil biodegradation (Lee et al., 1996). OMA generation has been estimated to initiate at concentrations of suspended sediment >10 mg/L for significant oil deposition and > 100 mg/L for large deposition events (Boehm, 1987; Daly et al., 2016).

The use of dispersants as an oil spill response method leads to the formation of small-droplet oil dispersions and remove the oil from the sea surface. Efficient treatment will result in oil and dispersant dilution in the water column, with the oil rapidly diluted to concentrations well below 1 mg/L (Lee et al., 2013; Prince et al., 2016). Dispersants are typically used in association with surface oil spills. However, during the DWH subsurface spill, dispersants were also injected at the wellhead to reduce oil surfacing, resulting in a deep-sea oil plume (Camilli et al., 2010; Reddy et al., 2012).

During the DWH spill, the oil sedimentation processes became associated with potential oil-related aggregates (ORAs) primarily by fall-out from the deep sea plume, but sedimentation was also suggested to originate from surfaced oil (Stout and Payne, 2016; Valentine et al., 2014). Experimental studies showed that ORAs from field-collected or laboratory-prepared oil samples resulted in oil sedimentation, although floating aggregates were also observed (Passow and Ziervogel, 2016; Passow et al., 2012). Both oil-degrading bacteria and oil-diatom coagulation seemed to be involved in the ORA formation processes (Passow et al., 2012). Since the oil spill site was not far from the Mississippi delta, and the river outflow became strong during the spill period, suspended sediment particles transported by the river was also likely to interact with the oil and may have contribute to oil sinking (Kourafalou and Androulidakis, 2013; Vonk et al., 2015).

Several research projects have been performed recent years, to try to understand the processes associated with the formation of oil-related aggregation. Most of these studies have been performed at high oil concentrations, e.g. 0.6% to 1% oil, corresponding to 600–10,000 mg/L oil (Passow et al., 2012; Ziervogel et al., 2012; Fu et al., 2014; Passow, 2016). Algal aggregates may carry up to 40% of the aggregated organic carbon as dispersed oil (Passow et al., 2019). While oleophilic oil compounds are incorporporated in the aggregates by droplet integration, more soluble compounds may become associated by sorption after dissolution from the oil droplets (Wirth et al., 2018).

In this study, we investigated the impacts of different phytoplankton species, mineral particle concentrations, oil concentrations on formation and fate of ORAs in temperate SW relevant for summer conditions in the North Sea and Norwegian Sea, an area with extensive offshore oil production and transport. Although most ORA-related studies have been performed at conditions relevant for the Gulf of Mexico, we expected the same processes to be relevant also for colder SW, including impacts of phytoplankton species and mineral particles on oil aggregation processes. Most importantly, we expected that the oil droplet dilutions caused by the dispersant treatment would significantly impact the ORA formation.

## 2. Materials and methods

### 2.1. Seawater, phytoplankton and mineral particles

The SW used in this study was collected from a depth of 80 m (close to the seabed) in the local fjord outside the harbour area of Trondheim, Norway (63°26′N, 10°24′E). The SW is directly supplied to the laboratories of SINTEF Ocean though a polyethylene pipeline system. The depth of the pipeline inlet is well below the thermocline, securing a stable temperature of 6–8 °C all the year around (Brakstad et al., 2004). The SW has a salinity of 34‰, and the water source is considered to be non-polluted and not influenced by seasonal variations. The SW passes a sand filter to remove coarse particles, before entering our laboratories. Recent studies showed mineral nutrient concentrations in the SW of 19 μg/L total-P, 16 μg/L *o*-$PO_4$-P, 130 μg/L $NO_2$ + $NO_3$-N, and 3 μg/L $NH_4$-N, and < 0.05 mg/L Fe (Brakstad et al., 2015).

Four batch cultures of phytoplankton were included in this study, all representing abundant genera in the North Sea and Norwegian Sea (Degerlund and Eilertsen, 2010; Vaulot et al., 2008). *Thalassiosira rotula* Meunier (clone RCC290, Roscoff Culture Collection, Roscoff, France) and *Skeletonema pseudocostatum* (clone NIVA-Bac 1, NIVA Culture Collection, Oslo, Norway) are chain-forming diatoms regarded as autotrophic (Fig. S1, Supplementary Material 1). *Phaeocystis globosa* (strain RA080513–08, Roscoff Culture Collection) represents a polymorphic coccoid life cycle, ranging from free-living cells to large colonies (Fig. S1). *Micromonas pusilla* (strain MICROVIR 1CR_2, Roscoff Culture Collection) is a flagellar picophytoplankton (< 2 μm in diameter; Fig. S1). *S. pseudocostatum* was cultured in 20% of a Z8 medium (Skulberg and Skulberg, 1990) in sterile-filtered SW (0.2 μm), while *T. rotula*, *P. globosa* and *M. pusilla* were cultured in K + Si-, K/2ET- and K-media, respectively (http://roscoff-culture-collection.org/culture-media). All media were sterile-filtered (0.2 μm) before inoculations. The phytoplankton cultures were incubated at 15 °C or 20 °C (see Table S1, Supplementary Material 1) under constant light conditions (60–120 μE/s/$m^2$) for 10–17 days, and cell concentrations determined in a Bürker haemocytometer for *S. pseudocostatum* and *T. rotula*, and by Coulter Counter analyses for *P. globosa* and *M. pusilla* (Table S1).

Commercially available diatomaceous earth (Celite 512, Sigma-Aldrich), reported by the supplier to have a median particle size 16 μm and a density of 2.2 g/$cm^3$, was used as mineral particles in the experiment.

### 2.2. Oil-dispersion stock solution

All ORAs were generated by using dispersed fresh naphthenic Troll C oil (batch 2007-0087); (density of 0.900, pour point of −18 °C, asphaltene content of 0.2 wt%, and wax content of 2.0 wt%) and Corexit 9500A (Nalco, Sugar Land, TX, USA). The oil dispersion stock solutions were prepared with the SINTEF oil droplet generator (Nordtug et al., 2011). Oil dispersions with pre-defined oil droplet size distributions and concentrations are generated by injecting oil via a capillary into a flow of SW which moves through three chambers (8 mm inner diameter) connected by nozzles with diameter of 0.5 mm (Nordtug et al., 2011). Stock dispersions were prepared, pre-determined for oil droplet concentrations of 600 mg/L, and with median droplet sizes close to 10 μm, as measured by Coulter Counter analyses (Fig. S2, Supplementary Material 2).

### 2.3. Microcosm setup

Pyrex flasks (1.1 L; Schott) were customized to a flat shape by a local glassblower (Faculty of Natural Sciences, Norwegian University of Science and Technology) and pre-treated as previously described (Brakstad et al., 2015). The flasks were filled with natural SW (unfiltered) and acclimated to 13 °C for 24 h, leaving approximately 50 mL headspace for adding oil dispersion stock solution, phytoplankton and mineral particles.

Flasks were mounted and incubated in a low-energy carousel system. The system consists of wheels slowly rotating around the carousel axis (0.75 r.p.m.) by a gear motor (Brakstad et al., 2015).

#### 2.3.1. Experiment with phytoplankton strains

In an experiment with different phytoplankton strains, volumes of algal cultures were inoculated in natural SW from late exponential or stationary growth phases to achieve final concentrations of $1 \times 10^4$ cells/mL, based on the determined phytoplankton concentrations (Table S1). Dispersed oil was applied to temperature-acclimated (13 °C) SW from the stock dispersions (600 mg/L; median droplet sizes ~10 μm) to a final concentration of 15 mg/L oil. The flasks were then completely filled with natural SW. Flasks with oil dispersions in SW with 50 mg/L $HgCl_2$, and without phytoplankton, were also included (sterilized controls). All flasks were tightly sealed, mounted in the carousel system and incubated in darkness at 13 °C in a temperature-controlled room for 21 days, and with constant rotation. Phytoplankton aggregation in the presence of the oil dispersions were determined by silhouette camera (SilCam) analyses after 1, 3, 5, 7, 10, 14 and 21 days of incubation (triplicate analyses).

#### 2.3.2. Experiment with different concentrations of diatomaceous earth

An experiment was performed with diatomaceous earth (Celite 512) at different concentrations, in the presence of oil dispersions and a phytoplankton culture. Dispersed oil from a stock solution (600 mg/L; median droplet size ~10 μm) and *S. pseudocostatum* from a late exponential/stationary phase growth culture (incubated for 12 days at 20 °C; algal concentrations $5.3 \times 10^6$ cells/mL) was added to flasks with temperature-acclimated (13 °C) SW at final concentrations of 15 mg/L oil dispersions and $1 \times 10^4$ cells of the phytoplankton culture. Diatomaceous earth was applied at final nominal concentrations of 5 mg/L, 10 mg/L or 30 mg/L. The flasks were completely filled with natural SW, mounted in the carousel system, and incubated in darkness at 13 °C (temperature-controlled room) for 14 days with constant rotation. Some controls were also incubated with oil dispersions and phytoplankton culture, but without diatomaceous earth. All flasks were tightly sealed before incubation. Aggregation related to concentrations of diatomaceous earth was determined by SilCam analyses after 1, 2, 5, 6, 10 and 14 days of incubation (triplicate analyses).

#### 2.3.3. Experiment with different concentrations of oil dispersions

An oil droplet stock solution was applied in different volumes to flasks with temperature-acclimated (13 °C) SW containing *S. pseudocostatum* at final concentrations $1 \times 10^4$ cells/mL (diluted from a late exponential growth culture incubated for 10 days at 20 °C; algal concentrations $5.5 \times 10^6$ cells/mL) and 5 mg/L diatomaceous earth, and the flasks were then filled completely with SW. The nominal concentrations of oil dispersions were 10 mg/L, 1 mg/L, 0.1 mg/L or 0.01 mg/L. Some flasks with phytoplankton and diatomaceous earth in SW, but without oil, were included as controls. All flasks were tightly sealed, mounted in the carousel system and incubated in darkness at 13 °C (temperature-controlled room) for 21 days with constant rotation. Aggregation related to concentrations of dispersed oil was determined by SilCam analyses after 0, 1, 5, 10, 14 and 21 days of incubation (triplicate analyses). Samples collected at the start and end of the incubation (0 and 21 days) were sampled for oil compound group analyses (see sct. 2.5).

### 2.4. Silhouette camera analyses

Aggregation during the experiments was monitored by non-destructive SilCam analyses (SINTEF SilCam) to document changes in particle size distribution (PSD) for particles >100 μm. Flasks were positioned in front of the camera, and recording was started immediately after they were slowly flipped to an upright position. Images are acquired in colour at 15 Hz for about 60 s for each sample (Davies et al., 2017). The images were processed, and particle size distributions were described by the particle volume distribution per equivalent circular diameter (ECD), reported as median diameter (D50) in each sample.

### 2.5. Sampling and oil compound group analyses

Sampling for chemical analyses in the experiment with different oil concentrations (sct. 2.3.3) was performed at day 0 (after 30 min on the carousel) and after 21 days incubation (triplicate samples) in the experiment with different concentrations of dispersed oil. Samples (1.1 L) were filtered through a steel filter with 20 μm mesh size (Teichhansel Teichshop/Siebgewebeshop; Bockhorn, Germany) using gravimetric force to capture aggregates on the filter surfaces. Thus, ORAs were defined in the experiments reported here as particles with a diameter > 20 μm. Biofilms attached to the glass wall were released by careful shaking prior to filtration. The steel filters were then extracted in dichloromethane (DCM) for chemical analyses, while the flow-through from each steel filter was acidified with 15% HCl to pH < 2 and subject to solvent-solvent extraction with DCM.

Oil compound analyses of DCM extracts included total extractable organic material (TEM), quantified by GC-FID analyses (Agilent 6890 N) gas chromatograph with a 30 m Durabond DB1 column; Agilent Technologies with an Agilent 7683B automatic injection system and a flame ionization detector. *O*-Terphenyl (10 mg/mL) was used as surrogate internal standard (SIS), and 5α-androstane as recovery internal standard (RIS). GC–MS analyses of 96 individual targeted compound or compound groups in the semi-volatile organic carbon (SVOC) fraction included quantification of *n*-alkanes ($nC_{10}$-$nC_{36}$), decalins ($C_0$- to $C_4$-alkylated), phenols ($C_0$- to $C_5$-alkylated), naphthalenes ($C_0$- to $C_4$-alkylated), 2- to 6-ring polycyclic aromatic hydrocarbons (PAH) and 17α(H),21β(H)-hopane. The GC–MS analyses were performed with an Agilent 6890 plus GC coupled with an Agilent 5973 MSD detector, operated in selected ion monitoring (SIM) mode. The GC was fitted with a HP-5MS 60 m fused silica capillary column. Deuterated SIS-PAH (naphthalene, phenanthrene, chrysene, perylene; 50–250 μg/mL) and RIS-PAH (acenaphthene, fluorene; 100 μg/mL) were included for analyses. Response values for individual target analytes in the GC–MS analyses were determined based on a signal-to-noise ratio of >10, with a limit of detection (LOD) set to 0.01 μg/L for individual oil compounds. Experimental blanks (deionized water) and a QA oil spike (a standard fresh paraffinic oil) were included in analyses of all test batches for GC-FID and GC–MS analyses. In addition, a QA PAH spike was included in all GC–MS test batches. Target compounds were normalized against the biomarker 17α(H),21β(H)-hopane (Prince et al., 1994).

### 2.6. Other analyses

Concentrations of oil droplets within the diameter range 2.6 to 60 μm were analysed by a Multisizer 4 Coulter Counter, fitted with a 100 μm aperture (Beckman Coulter Life Sciences, Indianapolis, IN, USA), using filtered SW (0.22 μm) as an electrolyte.

Dissolved oxygen (DO) was determined by a DO meter (Model 59 Dissolved Oxygen Meter, YSI Inc., Yellow Springs, OH, USA).

*t*-tests (paired or unpaired) and one-ways ANOVA analyses were performed by GraphPad Prism version 6.1 (GraphPad Software, San Diego, CA, USA).

## 3. Results and discussion

### 3.1. ORA formation in relation to phytoplankton species

In the current study, aggregate formation was compared in temperate SW (13 °C) with dispersed oil (15 mg/L), and in the presence of each of the four phytoplankton species *T. rotula*, *S. pseudocostatum*, *P. globosa* and *M. pusilla*. The phytoplankton concentrations used were relevant for a typical North Sea algal bloom (Gieskes and Kraay, 1986). Aggregate sizes were measured by SilCam analyses. The median aggregate sizes (d50) in the samples with the four phytoplankton species ranged between 144 ± 33 μm to 445 ± 405 μm at the start of the experiment (d0), but increased over time for *T. rotula*, *S. pseudocostatum* and *P. globosa*. However, aggregate sizes of *M. pusilla* decreased over time (Fig. 1). After 21 days of incubation, the largest median aggregates were formed by *P. globosa* (1682 ± 688 μm), compared to 1167 ± 233 μm by *T. rotula* and 1107 ± 556 μm by *S. pseudocostatum* (Fig. 1). The typical variable particle sizes resulted in high standard deviations, and the aggregate sizes were not significantly different between the three species ($P > 0.05$; one-way ANOVA).

While three of the species included in this study (*T. rotula*, *S. pseudocostatum* and *P. globosa)* have been reported to produce TEP essential for phytoplankton-related ORA formation (Passow, 2002; Dutz et al., 2005; Fukao et al., 2010), TEP production by *M. pusilla* has only been associated with viral infections of the cells (Lønborg et al., 2013). In our experiment, no viral trigger of TEP formation seemed to be present in this species. It should also be noted that previous studies have shown ORA formation in SW without phytoplankton (Bælum et al., 2012; Hazen et al., 2010; Netzer et al., 2018), associated with bacterial communities forming sticky extracellular polymeric substances (Fu et al., 2014; Gutierrez et al., 2018).

Common bloom phytoplankton species like *T. rotula* and *S. pseudocostatum* are chain-forming diatoms, while *P. globosa* is a marine haptophyte with a complex polymorphic life cycle between different types of free-living cells and gelatinous colonies during massive blooms (Schoemann et al., 2005). Although continuous increases of particle sizes were observed during the incubation period with these species, phytoplankton-associated aggregates are known to be fragmented in the SW column by zooplankton predation and bacterial degradation (Alldredge and Silver, 1988), but were reported to resist abiotic fragmentation by fluid shear (Alldredge et al., 1990).

A small aggregation was also measured in the sterilized controls without phytoplankton (Fig. 1), indicating the possibility for physical aggregation, for instance caused by oil droplet coalescence. The buoyancy of the ORAs during the experiment was variable and showed no clear trend over time or type of algae strain. At all timepoints some aggregates were rising, sinking or neutrally buoyant.

### 3.2. ORA formation and concentrations of diatomaceous earth

Diatomaceous earth was used as mineral particles in these studies. Although diatomaceous earth is of biogenic origin, the particles are inorganic and are constituted of opaline silica ($SiO_2 \cdot nH_2O$) from diatoms (Goldberg, 1958), representing a fraction of the autochthonous particles in the marine environment. Coulter Counter measurements of commercially available diatomaceous earth (Celite 512) showed a median particle size of 12 μm (Fig. S3, Supplementary Material 2), i.e. a smaller size than reported by the supplier (16 μm). A nominal concentration of 5 mg/L diatomaceous earth resulted in a volumetric concentration of $1.882 \times 10^6$ $\mu m^3$/mL (Fig. S3) and a measured concentration of 4.1 mg/L (based on a reported density of 2.2 g/$cm^3$). The impact of Celite concentrations on aggregation was determined in the presence of oil dispersions (15 mg/L) and a culture of *S. pseudocostatum* in late exponential growth phase. While the dispersed oil and phytoplankton stimulated ORA formation after 14 days of incubation at 13 °C, from 158 ± 39 μm at d0 to 870 ± 115 μm at d14, the presence of Celite at 5 mg/L further increased aggregate sizes, from 595 ± 56 μm at d0 to 2536 ± 2074 μm at d14 (Fig. 2). However, due to the large standard deviations, the median aggregate sizes at d14 did not differ significantly between the treatments with and without Celite ($P > 0.05$; unpaired test). Introduction of higher Celite concentrations (10 mg/L and 30 mg/L) did not increase aggregate sizes compared to dispersions without mineral particles (Fig. 2).

Concentrations of suspended mineral particles in SW may vary considerable spatially and temporally, from several grams per L water in estuaries of large rivers (Li et al., 1999) to <1 mg/L in coastal and oceanic SW (Zhang et al., 2014). The Celite concentrations used in our studies therefore represented typical coastal rather than oceanic conditions. For OMA processes, the oil aggregation increases with mineral concentrations, and decreases with increased mineral particle sizes. OMA formation has typically proven efficient with sediments (kaolinite, montmorillonite, quartz and silica) at concentrations of 60 mg/L or more, and with median particle sizes of 1 μm or less (Ajijolaiya et al., 2006; Stoffyn-Egli and Lee, 2003). The Celite concentrations (5 mg/L to 30 mg/L) and particle size (median size of 12 μm) used in our experiments were therefore not expected to result in efficient OMA formation. Less than 1% of the Celite surface was represented by the particles with surface diameter < 1 μm or lower, based on Coulter

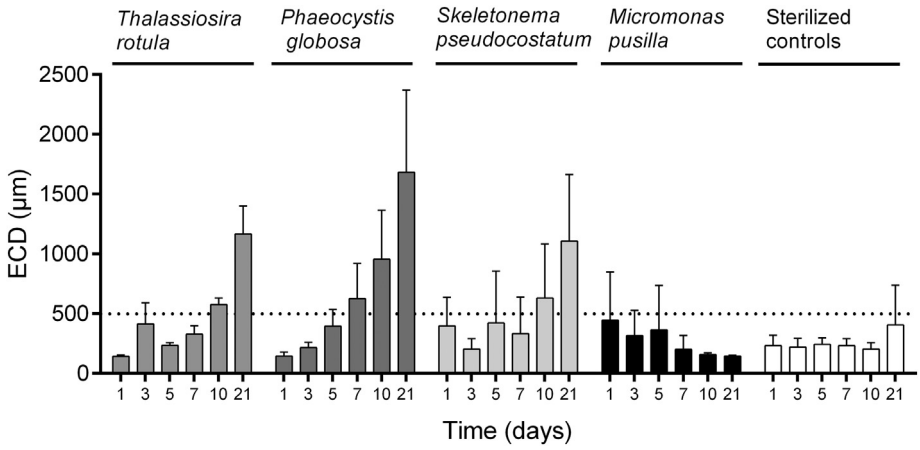


**Fig. 1.** ORA formation over time, given as equivalent circular diameter (ECD) of chemically dispersed oil (15 mg/L droplet concentrations) in natural SW incubated with different phytoplankton species (10,000 cells/ml) at 13° in the dark. Sterilized controls include dispersed oil in SW with $HgCl_2$ (50 mg/L). Error bars represent standard deviation of 3 replicates. The horizontal line at 500 μm shows the size limit of MarS aggregates (Alldredge et al., 2002).

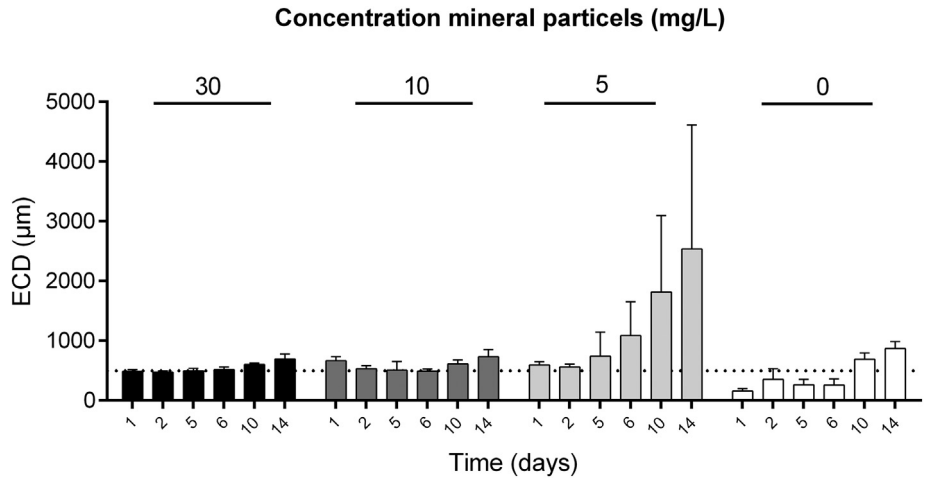


**Fig. 2.** ORA formation of 15 mg/L chemically dispersed oil over time in the presence of *S. pseudocostatum* (concentrations of 10,000 cells/mL), incubated at 13 °C in the dark at decreasing concentrations of mineral particles. Error bars represent standard deviation of 3 replicates. The horizontal line at 500 µm shows the size limit of MarS aggregates (Alldredge et al., 2002).

Counter determination (Fig. S3). Instead of contributing to OMA formation, Celite probably aided as a contributor to the aggregation caused by the phytoplankton culture. The ORAs are formed through interactions between oil and mucus-producing phytoplankton and bacteria, and mineral particles at low concentrations (5 mg/L) probably contributed to increased ORA sizes by their physical attachments to the aggregates. However, at higher concentrations of Celite (10 and 30 mg/L), excess of mineral particles may have saturated the sticky surfaces of the ORAs, reducing the stickiness and destabilizing the aggregates (Hamm, 2002). High concentration and large surface areas of Celite could also favour oil attachment to the mineral particles, inhibiting the contact between oil droplets and sticky phytoplankton particles.

In the presence of Celite, the aggregates were supplied with weighing material (specific gravity 2.1; information from the supplier), and the aggregates were observed to show mainly sinking behaviour, while aggregates of only oil and phytoplankton were mainly floating in the SW. In a recent study, we measured sinking velocities of ORAs in SW at 20 °C ranging from 50 to 200 m/days, both with and without Celite. However, at lower temperatures (13 °C and 5 °C), sinking properties of aggregates were reduced without Celite (Henry et al., 2020), in agreement with the results from the current study. In another study, aggregate sinking properties with dispersed oil and species of *Skeletonema* and *Thalassiosira* were also observed also at SW temperatures of 13 °C in the absence of mineral particles (Passow et al., 2019).

### 3.3. ORA formation with different oil concentrations

Since dispersed oil will be rapidly diluted in the SW column, an experiment was performed to determine the impact of oil dilution on aggregate formation and particle oil attachment. Dispersions were prepared in nominal oil concentrations of 10 mg/L to 0.01 mg/L oil, and in the presence of phytoplankton (*S. pseudocostatum*) and Celite, as described in the Materials and Methods. During an incubation period of 21 days (13 °C), aggregation was measured only at the higher oil concentration (10 mg/L), with median aggregate sizes increasing from 249 ± 47 µm at d0 to 3341 ± 637 µ, at d14, i.e. a size increase by a factor of 13 (Fig. 3). The corresponding factor of size increase from d0 to d14 at 1.0 mg/L oil was 1.7 (from 264 ± 41 µm to 417 ± 45 µm; Fig. 3). For the other oil concentrations (0.1 mg/L and 0.01 mg/L), the aggregate sizes increased from d0 to d14 by factors <1.2, which were similar to the factor of 1.3 determined in the vials without oil (Fig. 3). Only the aggregate sizes at 10 mg/L oil differed significantly from the values of without oil after 14 days of incubation ($P < 0.05$; unpaired *t*-tests). After 21 days of incubation, median aggregate sizes were significantly reduced from day 14 (factor of 4) in the 10 mg/L oil dispersions ($P < 0.05$; unpaired t-tests), probably as a result of aggregate disintegration. These results therefore showed that the oil was the main driver for formation of large aggregates in the experiments, and that concentrations >1 mg/L oil were required for major aggregate formation.

The TEM quantified by GC-FID analyses has been reported to represent more than 80% of most light oils, according to the true boiling point curve (Pasquini and Bueno, 2007), and measured TEM concentrations were mainly in agreement with nominal oil concentrations at the start of the experiment (d0) for the concentrations 10 mg/L, 1.0 mg/L and 0.1 mg/L (Table S2, Supplementary Material 3). However, the 0.01 mg/L concentration showed higher than expected concentrations, probably caused by the analytical uncertainties at this low oil concentration. After 21 days of incubation, the relative reductions of TEM concentrations compared to initial oil concentrations were 3% for 10 mg/L, 42% for 1.0 mg/L, 68% for 0.1 mg/L and 69% for 0.01 mg/L (Table S2). Oil associated with the ORA fractions was measured already at the start of the experiment. The ORA fraction of the oil at d0 increased by reduced oil concentration, from 7 ± 1% at 10 mg/L oil, to 38 ± 11% at 0.01% oil (Fig. 4). However, the fractions of TEM in the ORAs increased significantly ($P < 0.05$; paired t-test) during the experiment, representing 47–89% (average 62 ± 18%) after 21 days (Fig. 4). In a recent study, immediate integration of oil droplets in phytoplankton aggregates were reported, while sorption of water-soluble compounds occurred later (Wirth et al., 2018). We therefore assumed that the TEM fraction in the ORAs at d0 was caused by immediate oil droplet integration, while the high fraction of TEM in the ORAs at the end of the experiment represented by additional oil droplet integration and sorption of soluble compounds.

### 3.4. Depletion of oil compound groups in the ORAs

Depletion of oil compound groups were examined after normalization against the recalcitrant oil compound 17α(H),21β(H)-Hopane (Prince et al., 1994). Since the experiments were performed in closed flasks without headspace, no evaporation should occur. Comparison of normalized oil compound concentrations (sum of concentrations in water and ORA fractions) at the start and end (21 days) of the experiment showed near complete depletion of naphthalenes (> 97%) at all oil concentrations, while *n*-alkane and 2- to 3-ring PAHs were depleted by 75–93%. The depletion of 4- to 6-ring PAH and decalins were lower, ranging from 26 to 69% for the 4- to 6-ring PAHs and 47 to 83% for the decalins (Fig. 5). The depletion of PAHs and decalins at d21 increased by reduced initial oil concentrations (Fig. 5) and were significantly

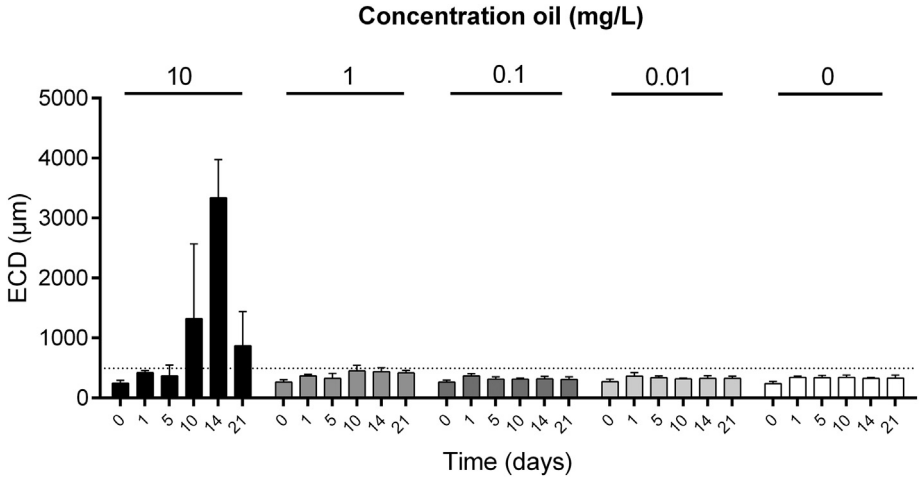


**Fig. 3.** ORA formation over time, given as equivalent circular diameter (ECD) of chemically dispersed oil with droplet concentrations of 10, 1, 0.1 and 0.01 mg/L, and without oil (0), incubated with phytoplankton (10,000 cells/ml) and mineral particles (5 mg/L) at 13° in the dark. Error bars represent standard deviation of 3 replicates. The horizontal line at 500 µm shows the size limit of MS aggregates (Alldredge et al., 2002).

different between the oil concentrations for both 2- to 3-ring PAHs, 4- to 6-ring PAHs and decalins ($P < 0.05$; one-way ANOVA analyses).

The depletion was mainly in agreement with biotransformation results from previous studies at 13 °C, in which TEM, *n*-alkanes and 2- to 4-ring PAHs were biotransformed by 58%, 96% and 97%, respectively (Brakstad et al., 2018). We therefore anticipate that the depletion in these experiments was mainly caused by microbial biotransformation. The biological activities at the higher oil concentrations were also confirmed by reductions of DO at the higher oil concentrations (Fig. S4, Supplementary Material 4), resulting in oxygen consumption of 4.7 mg/L at 10 mg/L oil, and 0.8 mg/L at 1 mg/L oil.

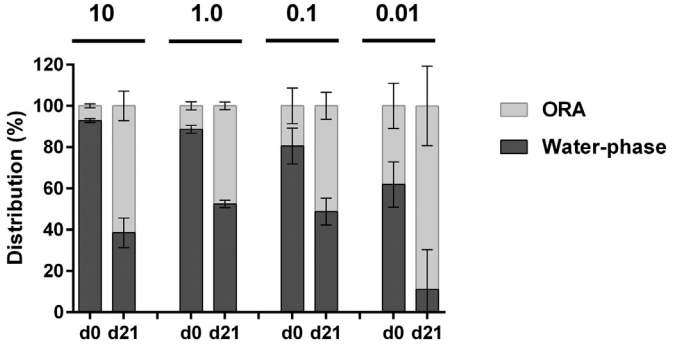


**Fig. 4.** Relative distributions of TEM in water-phases and ORAs at the start (d0) and after 21 days of incubation (d21) at 13 °C, and at nominal oil droplet concentrations of 10 mg/L, 1.0 mg/L, 0.1 mg/L and 0.01 mg/L. Error bars represent standard deviation of three replicates.

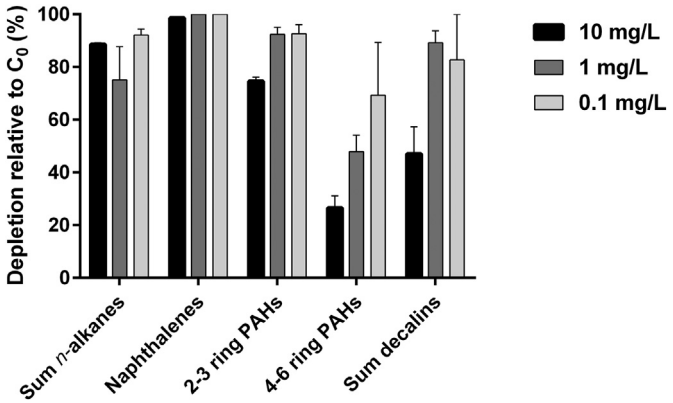


**Fig. 5.** Depletion of oil compound groups after 21 days of incubation relative to concentrations at the start of the experiment ($C_0$), shown as the sum of the compound groups in the water- and ORA fractions. The concentrations were normalized against 17α(H),21β(H)-Hopane. The error bars represent standard deviation of 3 replicates. Depletion of oil compounds at 0.01 mg/L oil was not determined, due to concentrations below LOD.

The relative distributions between ORA and SW fractions at days 0 and 21, showed that *n*-alkanes were rapidly integrated in the ORAs (d0), with ORA distributions increasing significantly ($P < 0.05$; one-way ANOVA) with decreasing oil concentration (22 ± 4% at 10 mg/L oil, 55 ± 9% at 1.0 mg oil and 76 ± 9% at 0.1 mg/L oil), as shown in Fig. 6A. Sorption of the sum of naphthalenes, PAHs and decalins occurred to a lesser extent at d0 (average 7 ± 2%; Fig. 6B) and did not differ significantly between the oil concentrations ($P > 0,05$; one-way ANOVA). The immediate concentration-dependent oil attachment of the ORAs (Fig. 4) may therefore be represented by poorly soluble alkanes, rather than more water-soluble naphthalenes and PAHs. Naphthalenes and smaller PAHs were probably rapidly dissolved from oil droplets. However, after 21 days of incubation, the relative fractions of both *n*-alkanes and the sum of naphthalenes, PAHs, and decalins increased, when compared to d0 (Fig. 6), ranging from 24% to 92% (average 61 ± 21%). However, the increases in ORA fractions from d0 to d21 were only significantly different for the naphthalenes/PAHs/decalins ($P < 0.05$, paired *t*-test), but not for the *n*-alkanes. This further substantiated that most of the *n*-alkanes were rapidly integrated in the ORAS as part of the oil droplets, while low-molecular weight naphthalenes and PAHs were rapidly dissolved from the oil droplets and subsequently sorbed by the aggregates (Wirth et al., 2018). Since most of the *n*-alkanes and the naphthalenes/PAHs/decalins were depleted after 21 days of incubation (Fig. 5), the soluble oil compounds in the water-phase were probably removed both by sorption to the ORAs and degradation, and with further degradation of oil compounds after particle sorption. This is in agreement with results from a recent study, showing faster oil compound depletion in the SW than in ORA fractions, since the oil compounds in the SW phase were both removed by biodegradation and accumulation into the aggregates. However, rapid biodegradation also occurred in the ORAs when the SW phase became emptied of oil compounds (Henry et al., 2020).

We did not separate between attachment of different oil compound groups to mineral particles and phytoplankton in this study. However, it has been estimated that both diatoms and mineral particles like diatomaceous earth may have considerable carrying capacity for dispersed oil (Passow et al., 2019; Wang et al., 2011; Özen et al., 2015; Farooqi, 2018).

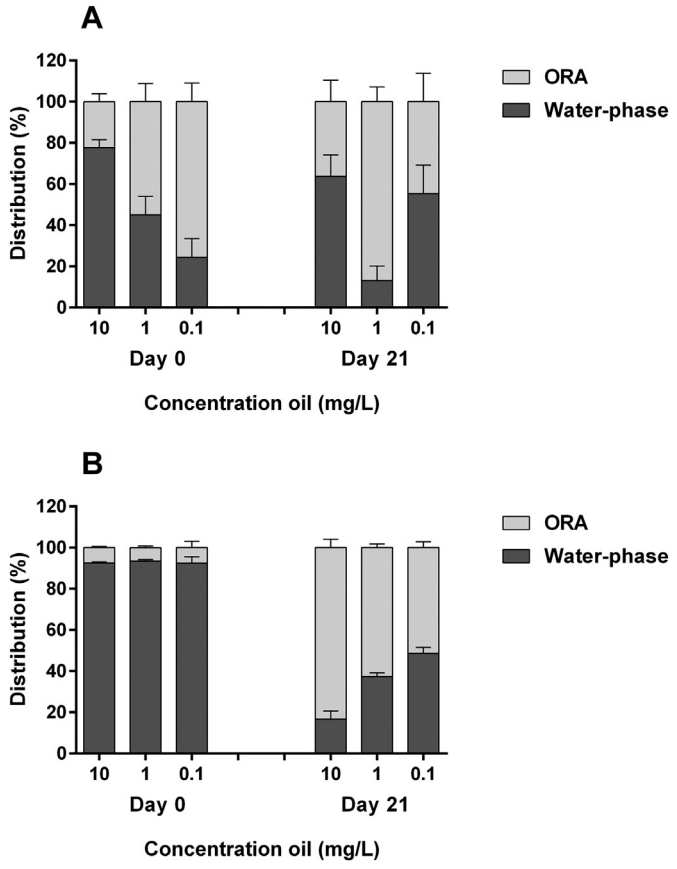


**Fig. 6.** Relative distribution between fractions of SW and ORAs of *n*C10-*n*C36 alkanes (A) and the sum of naphthalenes, decalins and 2- to 6-ring PAHs (B) at the start (day 0) and end (day 21) of the experiment. The error bars represent standard deviation of 3 replicates. Depletion of oil compounds at 0.01 mg/L oil was not determined, due to concentrations below LOD.

## 4. Conclusions

The results from these studies showed that dispersed oil may attach to small marine particles, but that the resulting processes and fate may depend on the oil concentrations. High oil concentrations may result in rapid aggregation and possible sedimentation through oil-related MarS processes, depending on TEP-producing phytoplankton and possible concentrations of mineral particles. The formed aggregates may sink to deeper water and sediment on the seabed (Stout and Payne, 2016; Passow et al., 2017; Passow et al., 2019). However, at lower concentrations of dispersed oil, as a result of droplet dilutions, the oil may attach to phytoplankton or mineral particles without aggregate formation and be transported with prevailing currents. Later particle aggregation and sedimentation by natural MarS processes may then result in oil sedimentation. However, since the attached oil is subject to continuous weathering processes like dissolution and biodegradation, only highly weathered and persistent oil fractions may end up on the seabed as result of these processes.

## CRediT authorship contribution statement

**Ingrid A. Henry:** Conceptualization, Data curation, Formal analysis, Investigation, Methodology, Resources, Software, Validation, Visualization, Writing - original draft, Writing - review & editing. **Roman Netzer:** Conceptualization, Data curation, Formal analysis, Methodology, Software, Supervision, Validation, Writing - review & editing. **Emlyn Davies:** Conceptualization, Data curation, Formal analysis, Investigation, Methodology, Software, Validation, Visualization, Writing - review & editing. **Odd Gunnar Brakstad:** Conceptualization, Data curation, Formal analysis, Funding acquisition, Investigation, Project administration, Resources, Supervision, Validation, Writing - original draft, Writing - review & editing.

## Declaration of competing interest

The authors declare that they have no known competing financial interests or personal relationships that could have appeared to influence the work reported in this paper.

## Acknowledgments

The research described in this paper was funded by the Research Council of Norway through the Petromaks2 program (contract #267767/E30), and the oil companies Equinor ASA and TOTAL E&P Norge ASA. Petroleum. We would like to thank Marianne Unaas Rønsberg, Inger K. Almås, Marianne Aas, Lisbet Støen and Lisbet Sørensen for chemical analyses and experimental assistance.

## Appendix A. Supplementary data

Supplementary data to this article can be found online at https://doi.org/10.1016/j.scitotenv.2020.141786.

## References

Ajijolaiya, L.O., Hill, P.S., Khelifa, A., Islam, R.M., Lee, K., 2006. Laboratory investigation of the effects of mineral size and concentration on the formation of oil–mineral aggregates. Mar. Pollut. Bull. 52, 920–927.

Alldredge, A.L., Silver, M.W., 1988. Characteristics, dynamics and significance of marine snow. Prog. Oceanograph. 20, 41–82.

Alldredge, A.L., Granata, T.C., Gotschalk, C.C., Dickey, T.D., 1990. The physical strength of marine snow and its implications for particle disaggregation in the ocean. Limnol. Oceanograph. 35, 1415–1428.

Alldredge, A.L., Cowles, T.J., MacIntyre, S., Rines, J.E.B., Donaghay, P.L., Greenlaw, C.F., Holliday, D.V., Dekshenieks, M.M., Sullivan, J.M., Zaneveld, J.R.V., 2002. Occurrence and mechanisms of formation of a dramatic thin layer of marine snow in a shallow Pacific fjord. Mar. Ecol. Prog. Series 233, 1–12.

Bælum, J., Borglin, S., Chakraborty, R., Fortney, J.L., Lamendella, R., Mason, O.U., Auer, M., Zemla, M., Bill, M., Conrad, M.E., 2012. Deep-sea bacteria enriched by oil and dispersant from the Deepwater Horizon spill. Environ. Microbiol. 14, 2405–2416.

Boehm, P.D., 1987. Transport and transformation processes regarding hydrocarbon and metal pollutants in offshore sedimentary environments. In: Boesch, D.F., Rabalais, N. (Eds.), Long-term Environmental Effects of Offshore Oil and Gas Development. Taylor and Francis, London, New York, pp. 233–286.

Brakstad, O.G., Bonaunet, K., Nordtug, T., Johansen, Ø., 2004. Biotransformation and dissolution of petroleum hydrocarbons in natural flowing seawater at low temperature. Biodegradation 15, 337–346.

Brakstad, O.G., Nordtug, T., Throne-Holst, M., 2015. Biodegradation of dispersed Macondo oil in seawater at low temperature and different oil droplet sizes. Mar. Pollut. Bull. 93, 144–152.

Brakstad, O.G., Farooq, U., Ribicic, D., Netzer, R., 2018. Dispersibility and biotransformation of oils with different properties in seawater. Chemosphere 191, 44–53.

Camilli, R., Reddy, C.M., Yoerger, D.R., Van Mooy, B.A.S., Jakuba, M.V., Kinsey, J.C., McIntyre, C.P., Sylva, S.P., Maloney, J.V., 2010. Tracking hydrocarbon plume transport and biodegradation at Deepwater horizon. Science 330, 201–204.

Daly, K.L., Passow, U., Chanton, J., Hollander, D., 2016. Assessing the impacts of oil-associated marine snow formation and sedimentation during and after the Deepwater horizon oil spill. Anthropocene 13, 18–33.

Davies, E.J., Brandvik, P.J., Leirvik, F., Nepstad, R., 2017. The use of wide-band transmittance imaging to size and classify suspended particulate matter in seawater. Mar. Pollut. Bull. 115, 105–114.

De La Rocha, C.L., Passow, U., 2007. Factors influencing the sinking of POC and the efficiency of the biological carbon pump. Deep Sea Res. Part II: Topical Studies Oceanograph. 54, 639–658.

Degerlund, M., Eilertsen, H.C., 2010. Main species characteristics of phytoplankton spring blooms in NE Atlantic and Arctic waters (68–80 N). Estuar. Coasts 33, 242–269.

Dutz, J., Breteler, W.K., Kramer, G., 2005. Inhibition of copepod feeding by exudates and transparent exopolymer particles (TEP) derived from a *Phaeocystis globosa* dominated phytoplankton community. Harmful Algae 4, 929–940.

van Eenennaam, J.S., Wei, Y., Grolle, K.C., Foekema, E.M., Murk, A.J., 2016. Oil spill dispersants induce formation of marine snow by phytoplankton-associated bacteria. Mar. Pollut. Bull. 104, 294–302.

Farooqi, H.N., 2018. Mixing of Diluted Bitumen and Conventional Crude Oil in Fresh and Marine Environments. Master Thesis at the Department of Chemical and Materials Engineering, University of Alberta, Edmonton, Canada. p. 195.

Fu, J., Gong, Y., Zhao, X., O'reilly, S., Zhao, D., 2014. Effects of oil and dispersant on formation of marine oil snow and transport of oil hydrocarbons. Environ. Sci. Technol. 48, 14392–14399.
Fukao, T., Kimoto, K., Kotani, Y., 2010. Production of transparent exopolymer particles by four diatom species. Fish. Sci. 76, 755–760.
Gieskes, W., Kraay, G., 1986. Analysis of phytoplankton pigments by HPLC before, during and after mass occurrence of the microflagellate Corymbellus aureus during the spring bloom in the open northern North Sea in 1983. Mar. Biol. 92, 45–52.
Goldberg, E.D., 1958. Determination of opal in marine sediments. J. Mar. Res. 17, 178–182.
Gutierrez, T., Teske, A., Ziervogel, K., Passow, U., Quigg, A., 2018. Microbial exopolymers: sources, chemico-physiological properties, and ecosystem effects in the marine environment. Front. Microbiol. 9, 1822.
Hamm, C.E., 2002. Interactive aggregation and sedimentation of diatoms and clay-sized lithogenic material. Limnol. Oceanograph. 47, 1790–1795.
Hazen, T.C., Dubinsky, E.A., DeSantis, T.Z., Andersen, G.L., Piceno, Y.M., Singh, N., Jansson, J.K., Probst, A., Borglin, S.E., Fortney, J.L., 2010. Deep-sea oil plume enriches indigenous oil-degrading bacteria. Science 330, 204–208.
Henry, I.A., Netzer, R., Davies, E.J., Brakstad, O.G., 2020. Formation and fate of oil-related aggregates (ORAs) in seawater at different temperatures. Mar. Pollut. Bull. 159, 111483.
Kourafalou, V.H., Androulidakis, Y.S., 2013. Influence of Mississippi River induced circulation on the Deepwater horizon oil spill transport. J. Geophys. Res.: Oceans 118, 3823–3842.
Lee, K., Weise, A.M., St-Pierre, S., 1996. Enhanced oil biodegradation with mineral fine interaction. Spill Sc. Technol. Bull. 3, 263–267.
Lee, K., Nedwed, T., Prince, R.C., Palandro, D., 2013. Lab tests on the biodegradation of chemically dispersed oil should consider the rapid dilution that occurs at sea. Mar. Pollut. Bull. 73, 314–318.
Li, B., Eisma, D., Xie, Q.C., Kalf, J., Li, Y., Xia, X., 1999. Concentration, clay mineral composition and coulter counter size distribution of suspended sediment in the turbidity maximum of the Jiaojiang river estuary, Zhejiang, China. J. Sea Res. 42, 105–116.
Lønborg, C., Middelboe, M., Brussaard, C.P., 2013. Viral lysis of Micromonas pusilla: impacts on dissolved organic matter production and composition. Biogeochem 116, 231–240.
Netzer, R., Henry, I.A., Ribicic, D., Wibberg, D., Brönner, U., Brakstad, O.G., 2018. Petroleum hydrocarbon and microbial community structure successions in marine oil-related aggregates associated with diatoms relevant for Arctic conditions. Mar. Pollut. Bull. 135, 759–768.
Nordtug, T., Olsen, A.J., Altin, D., Meier, S., Overrein, I., Hansen, B.H., Johansen, Ø., 2011. Method for generating parameterized ecotoxicity data of dispersed oil for use in environmental modelling. Mar. Pollut. Bull. 62, 2106–2113.
Özen, İ., Şimşek, S., Okyay, G., 2015. Manipulating surface wettability and oil absorbency of diatomite depending on processing and ambient conditions. Appl. Surface Sci. 332, 22–31.
Pasquini, C., Bueno, A.F., 2007. Characterization of petroleum using near-infrared spectroscopy: Quantitative modeling for the true boiling point curve and specific gravity. Fuel 86, 1927–1934.
Passow, U., 2002. Production of transparent exopolymer particles (TEP) by phyto-and bacterioplankton. Mar. Ecol. Prog. Series 236, 1–12.
Passow, U., 2016. Formation of rapidly-sinking, oil-associated marine snow. Deep Sea Research Part II: Topical Studies Oceanography 129, 232–240.
Passow, U., Ziervogel, K., 2016. Marine snow sedimented oil released during the Deepwater Horizon spill. Oceanograp 29, 118–125.
Passow, U., Ziervogel, K., Asper, V., Diercks, A., 2012. Marine snow formation in the aftermath of the Deepwater Horizon oil spill in the Gulf of Mexico. Environ. Res. Lett. 7, 035301.
Passow, U., Sweet, J., Quigg, A., 2017. How the dispersant Corexit impacts the formation of sinking marine oil snow. Mar. Pollut. Bull. 125, 139–145.
Passow, U., Sweet, J., Francis, S., Xu, C., Dissanayake, A., Lin, Y.-Y., Santschi, P., Quigg, A., 2019. Incorporation of oil into diatom aggregates. Mar. Ecol. Prog. Series 612, 65–86.
Prince, R.C., Elmendorf, D.L., Lute, J.R., Hsu, C.S., Haith, C.E., Senius, J.D., Dechert, G.J., Douglas, G.S., Butler, E.L., 1994. 17. alpha.(H)-21. beta.(H)-hopane as a conserved internal marker for estimating the biodegradation of crude oil. Environ. Sci. Technol. 28, 142–145.
Prince, R.C., Coolbaugh, T., Parkerton, T.F., 2016. Oil dispersants do facilitate biodegradation of spilled oil. PNAS 113, E1421.
Reddy, C.M., Arey, J.S., Seewald, J.S., Sylva, S.P., Lemkau, K.L., Nelson, R.K., Carmichael, C.A., McIntyre, C.P., Fenwick, J., Ventura, G.Y., Van Mooy, B.A.S., Camilli, R., 2012. Composition and fate of gas and oil released to the water column during the Deepwater Horizon oil spill. PNAS 109, 20,229–20,234.
Schoemann, V., Becquevort, S., Stefels, J., Rousseau, V., Lancelot, C., 2005. Phaeocystis blooms in the global ocean and their controlling mechanisms: a review. J. Sea Res. 53, 43–66.
Skulberg, O., Skulberg, R., 1990. Research with algal cultures. NIVA's culture collection of algae. Norwegian Institute for Water Research, Oslo, Norway.
Smetacek, V., 1985. Role of sinking in diatom life-history cycles: ecological, evolutionary and geological significance. Mar. Biol. 84, 239–251.
Stoffyn-Egli, P., Lee, K., 2003. Formation and characterization of oil–mineral aggregates. Spill Sci. Technol. Bull. 8, 31–44.
Stout, S.A., Payne, J.R., 2016. Macondo oil in deep-sea sediments: Part 1–sub-sea weathering of oil deposited on the seafloor. Mar. Pollut. Bull. 111, 365–380.
Valentine, D.L., Fisher, G.B., Bagby, S.C., Nelson, R.K., Reddy, C.M., Sylva, S.P., Woo, M.A., 2014. Fallout plume of submerged oil from Deepwater Horizon. PNAS 111, 15,906–15,911.
Vaulot, D., Eikrem, W., Viprey, M., Moreau, H., 2008. The diversity of small eukaryotic phytoplankton (≤3 μm) in marine ecosystems. FEMS Microbiol. Rev. 32, 795–820.
Vonk, S.M., Hollander, D.J., Murk, A.J., 2015. Was the extreme and wide-spread marine oil-snow sedimentation and flocculent accumulation (MOSSFA) event during the Deepwater Horizon blow-out unique? Mar. Pollut. Bull. 100, 5–12.
Wang, W., Zheng, Y., Li, Z., Lee, K., 2011. PIV investigation of oil–mineral interaction for an oil spill application. Chem. Engineer. J. 170, 241–249.
Wirth, M.A., Passow, U., Jeschek, J., Hand, I., Schulz-Bull, D.E., 2018. Partitioning of oil compounds into marine oil snow: insights into prevailing mechanisms and dispersant effects. Mar. Chem. 206, 62–73.
Zhang, X., Stavn, R.H., Falster, A.U., Gray, D., Gould Jr., R.W., 2014. New insight into particulate mineral and organic matter in coastal ocean waters through optical inversion. Estuar. Coast. Shelf Sci. 149, 1–12.
Ziervogel, K., McKay, L., Rhodes, B., Osburn, C.L., Dickson-Brown, J., Arnosti, C., Teske, A., 2012. Microbial activities and dissolved organic matter dynamics in oil-contaminated surface seawater from the Deepwater Horizon oil spill site. PloS one 7, e34816.